University of Dundee

An Efficient Finite Element Method with Exponential Mesh Refinement for the Solution of the Allen-Cahn Equation in Non-Convex Polygons

Celiker, Emine; Lin, Ping

Published in:
Communications in Computational Physics

DOI:
10.4208/CICP.OA-2020-0036

Publication date:
2020

Document Version
Peer reviewed version

Link to publication in Discovery Research Portal

Citation for published version (APA):
Celiker, E., & Lin, P. (2020). An Efficient Finite Element Method with Exponential Mesh Refinement for the Solution of the Allen-Cahn Equation in Non-Convex Polygons. *Communications in Computational Physics*, *28*(4), 1536-1560. https://doi.org/10.4208/CICP.OA-2020-0036

General rights
Copyright and moral rights for the publications made accessible in Discovery Research Portal are retained by the authors and/or other copyright owners and it is a condition of accessing publications that users recognise and abide by the legal requirements associated with these rights.

- Users may download and print one copy of any publication from Discovery Research Portal for the purpose of private study or research.
- You may not further distribute the material or use it for any profit-making activity or commercial gain.
- You may freely distribute the URL identifying the publication in the public portal.

Take down policy
If you believe that this document breaches copyright please contact us providing details, and we will remove access to the work immediately and investigate your claim.

Download date: 20. Apr. 2021

An Efficient Finite Element Method with Exponential Mesh Refinement for the Solution of the Allen-Cahn Equation in Non-Convex Polygons

Emine Celiker*[1] and Ping Lin*[2]

[1]School of Life Sciences, University of Lincoln, Joseph Banks Laboratories, Green Lane, Lincoln, LN6 7DL, UK
[2]Division of Mathematics, University of Dundee, 23 Perth Road, Dundee, Scotland, DD1 4HN, UK

Abstract

In this paper we consider the numerical solution of the Allen-Cahn type diffuse interface model in a polygonal domain. The intersection of the interface with the re-entrant corners of the polygon causes strong corner singularities in the solution. To overcome the effect of these singularities on the accuracy of the approximate solution, for the spatial discretization we develop an efficient finite element method with exponential mesh refinement in the vicinity of the singular corners, that is based on $(k-1)th$ order Lagrange elements, $k \geq 2$ an integer. The problem is fully discretized by employing a first-order, semi-implicit time stepping scheme with the Invariant Energy Quadratization approach in time, which is an unconditionally energy stable method. It is shown that for the error between the exact and the approximate solution, an accuracy of $O(h^k + \tau)$ is attained in the L^2-Norm for the number of $O(h^{-2}\ln h^{-1})$ spatial elements, where h and τ are the mesh and time steps, respectively. The numerical results obtained support the analysis made.

Keywords: Allen-Cahn equation, non-convex polygon, mesh refinement, corner singularities, finite element method, invariant energy quadratization, error estimation.

MSC 2010. 65M50, 65M60, 65M15, 65Z05

1 Introduction

It is well-known that the solutions of nonlinear diffusion equations which have very small diffusion coefficients or very large reaction terms often develop internal transition layers, called interfaces, that separate the spatial domain into different phase regions.

*Corresponding Authors: eceliker@lincoln.ac.uk, plin@dundee.ac.uk

First published in *Communications in Computational Physics* in volume 28, issue 4 (2020), published by Global Science Press.
© Global Science Press 2020.

Moreover, when these problems are posed in two-dimensional, non-convex polygonal domains, the solutions can also exhibit corner singularites. The classical finite-difference and finite element methods become ineffective around the singular corners and methods with special constructions are required for highly-accurate solutions, for which knowledge of the nature of the corner singularities becomes crucial.

An example of this is the Allen-Cahn equation introduced in [1], namely

$$u_t - \Delta u = \frac{1}{\epsilon^2} f(u), \tag{1.1}$$

which is a simple model of evolution of antiphase boundaries, where $\epsilon > 0$ is a small parameter and $f(u)$ is a bistable nonlinearity. The Allen-Cahn equation has been widely used to model various phenomena in nature. In particular, it has become a basic model equation for the diffuse-interface approach developed to study phase transitions and interfacial dynamics in material science [2]. Starting from arbitrary initial data, the solution of equation (1.1) develops interior layers, or interfaces. On one side of the interface, $u \sim u^+$ and on the other side $u \sim u^-$. The stable solution corresponds to an interface with a minimal perimeter that intersects the sides of the boundary orthogonally ([3], [4]).

Due to the nonlinearity in the equation, the solution of the Allen-Cahn equation can only be sought numerically. However, numerical methods regarding the solution of this equation have been largely considered in convex polygonal domains. To name a few of these studies, in [5] details were provided about the effectiveness of the high order and adaptive discretization schemes and the desirable choices of discretization parameters for simulations with very small interfacial width ϵ, a brief review and a critical comparison of the performance of several numerical schemes for solving the Allen-Cahn equation is presented in [6], and in [7] the error estimates for selected schemes with a spectral-Galerkin approximation for the numerical solution of the Allen-Cahn equation is analysed. However most of these methods cannot be directly applied in domains with re-entrant corners due to the possible low regularity of the solution at the intersection of the interface with the corners.

In this paper, we consider the numerical solution of the Allen-Cahn equation (1.1) in non-convex polygons. To overcome the effect of the corner singularities on the accuracy of the approximate solution, exponentially refined polar meshes are constructed in the vicinity of the corners of the polygon for the spatial finite element mesh. The proposed local mesh refinement is exponential in the polar radius r, uniform in the polar angle θ, and connected with the mesh in the remainder of the domain so that no additional techniques are required for coupling the solution in the subdomains. We obtain the numerical solution on the constructed mesh by using the finite element method based on $(k-1)th$ order Lagrange elements in space, $k \geq 2$, for all $t \geq 0$.

To fully discretize the problem, we consider the use of an unconditionally energy stable scheme for the time-stepping discretization. When the underlining energy law is stable in the fully discretized equation, it is generally possible to use a relatively coarse mesh in the simulation. Consequently such a method can reduce the cost of computation. Some energy stable temporal approximation methods include a second-order energy scheme introduced in [8] for a hydrodynamic phase-field model of binary fluid mixtures, the Scalar Auxiliary Variable approach presented in [9] as an energy stable scheme for a large class of gradient flows, and the modified second-order backward differentiation formula (BDF2) developed in [10] for the square phase-field crystal equation. Further studies on energy stable temporal schemes for the Cahn-Hilliard equation are also presented in [11]-[13].

In this paper, for the time discretization we employ a first-order, semi-implicit time stepping scheme with the Invariant Energy Quadratization (IEQ) approach. The IEQ Method, which is unconditionally energy stable, was first introduced in [14], and was applied for the Allen-Cahn equation in [15]. This is an efficient method since it requires the solution of a system of linear equations at each time step, and its analysis can easily be extended to a second-order scheme.

Finally we consider the error estimation of the developed method, and analyze the use of the refined mesh, as well as the application of a first-order time stepping scheme with the IEQ approach for the finite element solution of the problem. We show that the error between the solution obtained from the fully discretized problem and the exact solution has an accuracy of $O(h^k + \tau)$ in the L^2-norm for the number of $O(h^{-2} \ln h^{-1})$ spatial elements, where h, τ are the mesh and time steps, respectively, and $k \geq 2$ is an integer. The numerical results obtained support the theoretical analysis made.

The obtained error bound is based on the simplifying assumption that the interface width ϵ is fixed. Letting $\epsilon \to 0$ would require either using a very small spatial mesh step or the application of a numerical technique such as adaptive mesh refinement for obtaining the nmerical solution at the interface [16]. Nevertheless, the approach we have taken is an efficient alternative to using adaptive mesh refinement in the case of fixed ϵ, as our aim is to obtain *a priori* error estimates.

The structure of the paper is as follows. In Section 2 we give the problem formulation. In Section 3 we provide some preliminary results related to the corner singularities in the solution of second-order differential equations in non-convex polygons. In Section 4 we describe the proposed method for computing the numerical solution of the introduced initial-boundary value problem. Section 5 is devoted to the error analysis of the method. In Section 6 we present the solutions of the numerical examples solved by the proposed method, and finally concluding remarks are given in Section 7.

2 Problem Statement

Let Ω be an open simply-connected polygon, γ_j, $j = 1, ..., N$, be its sides, including the ends, enumerated counter-clockwise, $\gamma = \cup_{j=1}^{N} \gamma_j$ is the boundary of Ω, $\overline{\Omega} = \Omega \cup \gamma$, and ω_j, $0 < \omega_j < 2\pi$, is the interior angle formed by the sides γ_{j-1} and γ_j ($\gamma_0 \equiv \gamma_N$). Furthermore, we denote by $P_j = \gamma_{j-1} \cap \gamma_j$ the $j-th$ vertex of Ω and by r_j, θ_j a polar system of coordinates with pole in P_j and the angle θ_j taken counter-clockwise from the side γ_j.

We consider the solution of the initial-boundary value problem

$$u_t - \Delta u = \frac{1}{\epsilon^2} f(u) \text{ in } \Omega \times (0,T], \tag{2.1}$$

$$\frac{\partial u}{\partial n} = 0 \text{ on } \gamma \times (0,T], \tag{2.2}$$

$$u(\mathbf{x},0) = u_0(\mathbf{x}) \text{ in } \Omega, \tag{2.3}$$

where $T > 0$ is a fixed positive time, $\Delta \equiv \partial^2/\partial x^2 + \partial^2/\partial y^2$, $\mathbf{x} = (x,y)$, $f(u) = -F'(u)$, with $F(u)$ a double-well potential of equal depth defined by

$$F(u) = \frac{1}{4}(1-u^2)^2$$

so that

$$f(u) = u(1-u^2), \tag{2.4}$$

and ϵ is a prescribed positive constant.

It is easy to see that the function f satisfies the inequality

$$|f'(u)| \leq C(1+|u|^2), \tag{2.5}$$

where C is a positive constant.

We assume that the required compatibility conditions between the given boundary conditions and the initial data are satisfied on γ at $t = 0$, and the initial condition

$$u_0 \in H^k(\Omega),\ k \geq 2 \text{ an integer}, \tag{2.6}$$

where $H^m(S)$ is the Sobolev space equipped with the norms and seminorms

$$\|v\|_{m,S} = \left(\sum_{|\alpha| \leq m} \iint_S |D^\alpha v|^2 dS \right)^{1/2},$$

$$|v|_{m,S} = \left(\sum_{|\alpha| = m} \iint_S |D^\alpha v|^2 dS \right)^{1/2},$$

$m \geq 0$ an integer.

We also request the following regularity assumptions hold for the solution of problem (2.1)-(2.3):

$$u, u_t \in L^\infty(0,T;H^1(\Omega)) \tag{2.7}$$

$$u_{tt} \in L^2(0,T;H^1(\Omega)). \tag{2.8}$$

Throughout the paper the parameter k, $k \geq 2$, will have the same value, which also corresponds with the regularity assumption (2.6) of the initial condition.

3 Preliminaries

Corner singularities of various magnitudes often arise in the solutions of elliptic and parabolic differential equations in polygonal domains. For instance, consider the solution of the boundary value problem of Laplace's equation, which is a linear elliptic equation, in the neighbourhood T_j, $1 \leq j \leq N$, of the $j-th$ vertex of the polygonal domain Ω defined in Section 2:

$$\Delta v = 0 \text{ in } T_j \tag{3.1}$$

$$\frac{\partial v}{\partial n} = 0 \text{ on } \Gamma_1 \cup \Gamma_2, \ v = g \text{ on } \Gamma_3, \tag{3.2}$$

where $T_j \subset \Omega$ is a sectorial domain with radius r_0 defined by

$$T_j = \{(r_j, \theta_j) : 0 < r_j < r_0, 0 < \theta_j < \omega_j\}.$$

The rectilinear parts Γ_1 and Γ_2 of the boundary of T_j coincide with the boundary γ of Ω, and the curvilinear part Γ_3 lies inside Ω. The variables r_j, θ_j are defined as in Section 2 and the function g in (3.2) is a known smooth function.

By the method of separation of variables, the asymptotic expansion of the solution can be represented as

$$v(r_j, \theta_j) = \sum_{m=0}^{\infty} a_{jm} r_j^{\alpha_{jm}} \cos \alpha_{jm} \theta_j,$$

where $\alpha_{jm} = m\pi/\omega_j$ and the coefficients a_{jm} are determined by the boundary data on Γ_3.

It can be easily observed that

$$\frac{\partial v}{\partial r_j} = O(r_j^{\pi/\omega_j - 1}) \to \infty \text{ as } r_j \to 0 \tag{3.3}$$

when $\pi < \omega_j \leq 2\pi$, and hence the solution has a strong singularity at re-entrant corners, [17].

The equality (3.3) holds for the solutions of all linear elliptic and parabolic differential equations. However, a real corner theory for nonlinear problems does not exist. Nevertheless, there is no doubt that a singular expansion holds in all cases [18].

Next, consider the solution of the corresponding elliptic boundary value problem to problem (2.1)-(2.3) on T_j, $1 \leq j \leq N$:

$$-\Delta w = \frac{1}{\epsilon^2} f(w) \text{ on } T_j \tag{3.4}$$

$$\frac{\partial w}{\partial n} = 0 \text{ on } \Gamma_1 \cup \Gamma_2, \ w = g_w \text{ on } \Gamma_3. \tag{3.5}$$

We apply the transformation

$$r_j^{\epsilon} = r_j/\epsilon \tag{3.6}$$

to (3.4), (3.5), so that at the intersection of the interface with the $j-$th corner of Ω we have

$$-\Delta w_\epsilon = f(w_\epsilon) \text{ on } T_j^\epsilon \tag{3.7}$$

$$\frac{\partial w_\epsilon}{\partial n} = 0 \text{ on } \Gamma_1^\epsilon \cup \Gamma_2^\epsilon,\ w_\epsilon = g_w^\epsilon \text{ on } \Gamma_3^\epsilon. \tag{3.8}$$

where g_w^ϵ is a known, non-constant function, and T_j^ϵ is the transformation of T_j by (3.6).

As stated in [18], for the solution of the boundary-value problem (3.7), (3.8) the following sequence of theoretical results are accepted to hold in T_j^ϵ:

1. Existence of a weak solution w_ϵ,
2. Estimates of the Hölder exponent of the solution:

$$|w_\epsilon| \leq c(r_j^\epsilon)^{\alpha_j}, |\nabla w_\epsilon| \leq c(r_j^\epsilon)^{\alpha_j - 1},\ \text{etc.}, \tag{3.9}$$

   where c is a constant,

3. Existence of a decomposition

$$w_\epsilon = q_j s_j + h_j \tag{3.10}$$

   with singular function(s) s_j, where q_j is a coefficient and the remainder part h_j is more regular than s_j.

Hence it follows that on T_j,

$$|w| \leq c(r_j/\epsilon)^{\alpha_j}, |\nabla w| \leq c(r_j/\epsilon)^{\alpha_j - 1},\ \text{etc.}, \tag{3.11}$$

so that the corner singularity in the solution is restricted to the ϵ neighbourhood of the jth vertex of Ω.

4 Numerical Method

For the approximate solution of problem (2.1)-(2.3), we develop a numerical method based on the finite element method for the space discretization, and the Backward-Euler scheme with the Invariant Energy Quadratization (IEQ) approach for the time discretization, which is an unconditionally energy stable scheme.

We start by deriving the weak form of the initial-boundary value problem (2.1)-(2.3). Let us consider a smooth function $\varphi \in \mathcal{V}$, where $\mathcal{V} = H^1(\Omega)$.

The problem (2.1)-(2.3) is formulated in weak form as follows: Find $u \in \mathcal{V}$ such that for all $\varphi \in \mathcal{V}$

$$\int_\Omega \varphi \frac{\partial u}{\partial t} dx + \int_\Omega \nabla\varphi \nabla u dx = \frac{1}{\epsilon^2} \int_\Omega f(u)\varphi dx, \tag{4.1}$$

$$u(x, 0) = u_0(x). \tag{4.2}$$

For the approximation problem corresponding to (4.1), (4.2), we construct a finite element mesh in the domain Ω to be employed at each $t \in (0, T]$, with exponentially compressed meshes in the vicinity of the corners. A similar version of the exponentially refined meshes was introduced in [19] and applied for the second-order finite-difference solution of the Laplace equation on polygons, as part of an overlapping domain-decomposition method. In [20] and [21], the method was extended to the fourth and sixth order, respectively, finite-difference solution of Laplace's equation in staircase polygons, and in [22] exponentially compressed polar meshes were employed as part of a finite element mesh for the highly accurate solution of the Helmholtz equation in arbitrary polygonal domains. In this paper we develop this mesh into a triangular finite element mesh, and analyse the application of a conforming finite element method for the $k-th$ order, $k \geq 2$, approximate solution of the nonlinear, time-dependent equation (2.1) on the constructed mesh.

To this end, in the neighbourhood of each vertex P_j, $1 \leq j \leq N$, we construct a fixed sector $S_j = S_j(r_{j0}) \subset \Omega$, where

$$S_j(r_{j0}) = \{(r_j, \theta_j) : 0 < r_j < r_{j0}, 0 < \theta_j < \omega_j\},$$

$r_{j0} \leq \min\{l_{j-1}, l_j\}$ denotes the radius of the sector, where l_j is the length of the side γ_j. The rectilinear sides of the boundary of S_j coincide with the sides γ_{j-1} and γ_j of Ω, and we also assume that $\bar{S}_n \cap \bar{S}_m = \emptyset$, $1 \leq n, m \leq N$, where $\bar{S}_j$ denotes the closure of S_j.

Since the singularity at the corner pollutes the finite element solution in an area larger than the $\epsilon-$neighbourhood of the corner, we take $r_{j0} > c_1 > c_0\epsilon$, where $c_0 > 1$, c_1 are fixed positive constants and ϵ is the width of the interface.

We let $\Omega^* = \Omega \backslash \left(\cup_{j=1}^{N} S_j \right)$. For the solution of the approximation problem of (4.1), (4.2) in Ω^*, a finite element mesh is formed using triangular elements. The solution is based on $(k-1)th$ order Lagrange elements, which are C^0-continuous, $\mathcal{P}_{k-1}$ finite elements. We introduce the parameter $0 < h < \epsilon/4$, which denotes the largest side in any element of the mesh on Ω^*, and let Ω_h^* denote the mesh formed on Ω^*.

In each sector $\bar{S}_j$, $1 \leq j \leq N$, a mesh with triangular and curved elements is constructed as follows. We consider the family of rays $\theta_{jp} = p\beta_j$, $p = 0, 1, ..., \omega_j/\beta_j$ ($\omega_j/\beta_j \geq k$ an integer), with maximum angular step

$$\beta_j \leq h, \tag{4.3}$$

and the family of circles centered at P_j, with radii

$$r_{jq} = r_{j0} \exp(-q\beta_j), \; q = 0, 1, ..., \nu_j,$$

where

$$\nu_j = 1 + \left[\max\left\{ k, \frac{k \ln h^{-1}}{\beta_j \tilde{\alpha}_j} \right\} + N_{j0} \right], \tag{4.4}$$

with $\tilde{\alpha}_j > 0$ the Hölder exponent of the solution in S_j, $N_{j0} \geq 0$ is an arbitrary fixed number and $[\cdot]$ indicates the integer part. The choice of ν_j is justified in Section 5.

For the construction of the mesh, trapezia are formed using the intersection points of the rays and the family of circles defined above, and each trapezium is divided into two triangles avoiding obtuse triangles so that the mesh is compressed exponentially in the radial direction in S_j. Triangles with one curved side (curved elements) denoted t_c, are employed in the layer of elements adjacent to the arc $\vartheta_{j\nu_j} = (r_{j\nu_j}, \theta_j)$, $0 \leq \theta_j \leq \omega_j$, and are of the form described by Zlámal in [27]. The transformation introduced by Zlámal ([27]-[29]), namely

$$x = x^*(\zeta, \eta) \equiv x_1 + (x_2 - x_1)\zeta + (x_3 - x_1)\eta + (1 - \zeta - \eta)\Phi(\eta), \tag{4.5}$$

$$y = y^*(\zeta, \eta) \equiv y_1 + (y_2 - y_1)\zeta + (y_3 - y_1)\eta + (1 - \zeta - \eta)\Psi(\eta), \tag{4.6}$$

is used to map the unit triangle $\overline{\tau}_1$ with vertices $R_1(0,0)$, $R_2(1,0)$, $R_3(0,1)$ in the ζ, η-plane on the closed element t_c, where (x_i, y_i), $i = 1, 2, 3$, are the coordinates of the vertex Q_i of t_c, and Φ, Ψ are smooth functions with $\Phi(0) = \Psi(0) = 0$, that are constructed using the parametric equations of the curved side of t_c. As stated in [27], it will not be necessary to carry out the inversion $\zeta = \zeta(x, y)$, $\eta = \eta(x, y)$ in actual computations.

We denote by S_j^h the finite element mesh constructed on S_j, with boundary $\Upsilon_j = \bar{\gamma}_{j-1} \cup \bar{\gamma}_j \cup \hat{\vartheta}_{j0} \cup \vartheta_{j\nu_j}$, where $\hat{\vartheta}_{j0}$ denotes the union of the line segments joining the adjacent nodes on the arc of the circle lying inside Ω with radius r_{j0} and centre P_j, $\vartheta_{j\nu_j}$ is the arc defined above,

$$\bar{\gamma}_j = \{(r_j, \theta_j) : r_{j\nu_j} \leq r_j \leq r_{j0}, \theta_j = 0\},$$

$$\bar{\gamma}_{j-1} = \{(r_j, \theta_j) : r_{j\nu_j} \leq r_j \leq r_{j0}, \theta_j = \omega_j\},$$

and $\bar{S}_j^h = S_j^h \cup \Upsilon_j$.

The mesh Ω_h^* is chosen to be conforming with each $\bar{S}_j^h$, $1 \leq j \leq N$, so that no additional techniques are required to couple the solutions in the subdomains.

The exponentially refined mesh constructed in the vicinity of a re-entrant corner, with an interior angle of $3\pi/2$, is demonstrated in Figure 1.

The solution of the approximation problem on $\bar{S}_j^h$ will also be based on the $(k-1)th$ order Lagrange elements.

We let $\Omega_h \equiv \Omega_h^* \cup \left(\cup_{j=1}^N \bar{S}_j^h\right)$ denote the finite element mesh formed in Ω. Finally, let

$$\dot{\gamma}_j = \{(r_j, \theta_j) : 0 \leq r_j \leq r_{j\nu_j}, \theta_j = 0\},$$

$$\dot{\gamma}_{j-1} = \{(r_j, \theta_j) : 0 \leq r_j \leq r_{j\nu_j}, \theta_j = \omega_j\},$$

and $\dot{\gamma} = \cup_{j=1}^N (\dot{\gamma}_j \cup \dot{\gamma}_{j-1})$. Then the boundary of Ω_h is defined as $\gamma' = (\gamma \backslash \dot{\gamma}) \cup (\cup_{j=1}^N \vartheta_{j\nu_j})$.

We denote by $\mathcal{V}^h$ the finite element subspace of $\mathcal{V}$, defined by

$$\mathcal{V}^h = \{\varphi : \varphi \text{ is } C^0\text{-continuous}, \varphi \in \mathcal{P}_{k-1}(T) \text{ for each triangle } T \in \Omega_h\}.$$

Using the finite element method, the semi-discrete problem in space corresponding to (4.1), (4.2) may be stated as follows: Find $u_h \in \mathcal{V}^h$ such that for all $\varphi \in \mathcal{V}^h$

$$\int_{\Omega_h} \frac{\partial u_h}{\partial t} \varphi d\mathbf{x} + \int_{\Omega_h} \nabla u_h \nabla \varphi d\mathbf{x} = \frac{1}{\epsilon^2} \int_{\Omega_h} f(u_h) \varphi d\mathbf{x}, \tag{4.7}$$

$$u_h(0) = u_{h0}, \tag{4.8}$$

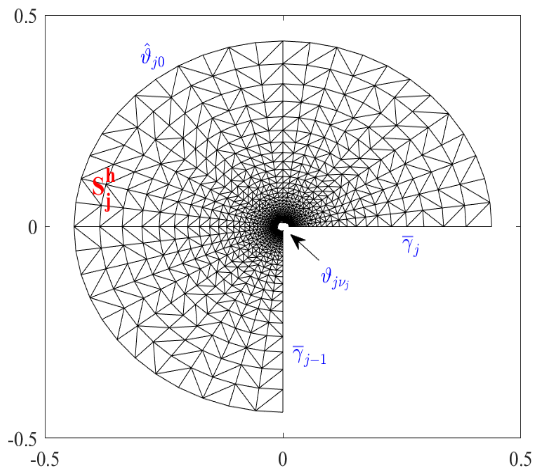

Figure 1: The exponentially refined mesh in the vicinity of the jth corner of a polygon, with $h = 2^{-4}$ and $\nu_j = 30$.

where u_{h0} is the $(k-1)th$ order orthogonal projection of u_0 onto $\mathcal{V}^h$. We assume homogeneous Neumann boundary conditions hold on the boundary γ' of the mesh Ω_h. It is clear that the problem (4.7), (4.8) has a unique solution defined for all time [23].

Remark 1. *For the implementation on the curved elements, the functions* Φ, Ψ *in (4.5), (4.6), respectively, can be approximated with the use of* $(k-1)th$ *order Lagrange polynomials of the parametric equations representing the curved side of* t_c*, [29].*

For the discretization of the time derivative in problem (4.7), (4.8), we employ a first-order semi-implicit method with the Invariant Energy Quadratization (IEQ) approach, which was introduced in [14]. This is an unconditionally energy stable scheme which is efficient to implement, since it requires the solution of a system of linear equations at each time step. For completeness, we provide more details of this method.

First, the Allen-Cahn equation (2.1) is recast in the following equivalent form:

$$u_t - \Delta u + \frac{1}{\epsilon^2}\mathcal{H}(u)\mathcal{U} = 0, \tag{4.9}$$

$$\mathcal{U}_t = \frac{1}{2}\mathcal{H}(u)u_t, \tag{4.10}$$

where $\mathcal{U}(u) = \sqrt{F(u)+1}$ and $\mathcal{H}(u) = \frac{-f(u)}{\sqrt{F(u)+1}}$. The functions f and F are defined as in (2.4). The initial and boundary conditions are the same as (2.2), (2.3), with the addition of the condition

$$\mathcal{U}|_{t=0} = \sqrt{F(u_0)+1}.$$

Using the Backward-Euler scheme for the time derivatives, the first-order, semi-discrete in time IEQ scheme for solving (4.9), (4.10) reads as follows:

$$\frac{u^n - u^{n-1}}{\tau} - \Delta u^n + \frac{1}{\epsilon^2}\mathcal{H}(u^{n-1})\mathcal{U}^n = 0, \tag{4.11}$$

$$\mathcal{U}^n - \mathcal{U}^{n-1} = \frac{1}{2}\mathcal{H}(u^{n-1})(u^n - u^{n-1}), \tag{4.12}$$

$$\partial u^n/\partial n|_\gamma = 0, \tag{4.13}$$

$$u^0 = u_0(\mathbf{x}),\ \mathbf{x} \in \Omega, \tag{4.14}$$

where τ denotes the time step and u^n is the solution at time $t_n = n\tau$.

The unconditional energy stability of the scheme (4.11)-(4.14) follows from Theorem 4.1 in [15].

For the implementation of the method, equations (4.11), (4.12) can be rearranged to a single equation in the form

$$\begin{aligned}\frac{1}{\tau}u^n - \Delta u^n + \frac{1}{2\epsilon^2}\mathcal{H}(u^{n-1})\mathcal{H}(u^{n-1})u^n &= \frac{1}{\tau}u^{n-1}\\ -\frac{1}{\epsilon^2}\mathcal{H}(u^{n-1})\left(\mathcal{U}^{n-1} - \frac{1}{2}\mathcal{H}(u^{n-1})u^{n-1}\right).\end{aligned} \tag{4.15}$$

From (4.7)-(4.8) and (4.15), we have the fully-discrete approximation problem to (4.1), (4.2) in the following weak form: For $u_h^{n-1} \in \mathcal{V}^h$ given, find $u_h^n \in \mathcal{V}^h$ such that for all $\varphi \in \mathcal{V}^h$

$$\frac{1}{\tau}(u_h^n, \varphi) + (\nabla u_h^n, \nabla\varphi) + \frac{1}{2\epsilon^2}((\mathcal{H}^{n-1})^2 u_h^n, \varphi) = (b^{n-1}, \varphi), \tag{4.16}$$

$$u_h(0) = u_{h0}, \tag{4.17}$$

where $b^{n-1} = \frac{1}{\tau}u_h^{n-1} - \frac{1}{\epsilon^2}\mathcal{H}^{n-1}\left(\mathcal{U}^{n-1} - \frac{1}{2}\mathcal{H}^{n-1}u_h^{n-1}\right)$, and $\mathcal{H}^{n-1} = \mathcal{H}(u_h^{n-1})$.

The well-posedness of the linear system (4.16), (4.17) follows from Theorem 4.2 in [15].

5 On the Error Bounds

For the analysis of the proposed method, we will require the *elliptic projection* R_h onto $\mathcal{V}^h$ defined as below, [24], [25].

Definition 1. *The elliptic projection R_h onto $\mathcal{V}^h$ is the orthogonal projection with respect to the inner product $a_h(w, \varphi) = (\nabla w, \nabla\varphi) + (w, \varphi)$, so that for $w \in \mathcal{V}$,*

$$a_h(R_h w - w, \varphi) = d(w, \varphi)\ \forall\varphi \in \mathcal{V}^h \text{ on } \Omega_h, \tag{5.1}$$

where

$$d(w, \varphi) = \sum_{j=1}^{N}\int_{\vartheta_{j\nu_j}} \frac{\partial w}{\partial r_j}(r_{j\nu_j}, \Theta)\varphi\ r_{j\nu_j} d\Theta. \tag{5.2}$$

Definition 1 may be expressed by saying that $R_h w \in \mathcal{V}^h$ is the finite element approximation of the solution to the corresponding elliptic problem with exact solution w, and as we are employing homogeneous Neumann boundary conditions on the boundary of Ω_h, the right-hand side term (5.2) follows from Green's theorem, [26].

In the analysis presented here it will be assumed that there exists a constant C such that

$$\left|\frac{\partial^k w}{\partial r_j^k}\right| \leq C r_j^{\tilde{\alpha}_j - k} \text{ in } S_j,\ 1 \leq j \leq N, \tag{5.3}$$

where $k \geq 2$, $\tilde{\alpha}_j > 0$, and

$$w \in H^k(\Omega^*). \tag{5.4}$$

Everywhere below we will denote constants which are independent of h and β by $c, c_0, c_1, \ldots$, generally using the same notation for different constants for simplicity.

We consider the upper bound of

$$\|w - R_h w\|_{0,\Omega_h}.$$

The coercivity and the continuity of the bilinear form $a_h(\cdot,\cdot)$ on $\mathcal{V}^h$ are trivial. Hence it follows from Lemma 10.1.7 in [26] that

$$\|w - R_h w\|_{0,\Omega_h} \leq c\left(\inf_{v\in\mathcal{V}^h}\|w - v\|_{0,\Omega_h} + \sup_{z\in\mathcal{V}_h/\{0\}}\frac{|a_h(w - R_h w, z)|}{\|z\|_{0,\Omega_h}}\right), \tag{5.5}$$

so that from Definition 1 we have

$$\|w - R_h w\|_{0,\Omega_h} \leq c\left(\inf_{v\in\mathcal{V}^h}\|w - v\|_{0,\Omega_h} + \sup_{z\in\mathcal{V}_h/\{0\}}\frac{|d(w, z)|}{\|z\|_{0,\Omega_h}}\right). \tag{5.6}$$

We first of all consider the first term on the right-hand side of inequality (5.6). Taking assumption (5.4) into account, it is straight forward to show by interpolation theory that

$$\inf_{\varphi\in\mathcal{V}^h}\|w - \varphi\|_{0,\Omega_h^*} \leq c_0 h^k,\ \forall\varphi\in\mathcal{V}^h. \tag{5.7}$$

Hence next we consider the error between the exact and the approximate solution on $\bar{S}_j^h$, $1 \leq j \leq N$. From interpolation theory and Theorem 2 in [27] for the curved elements,

$$\inf_{\varphi\in\mathcal{V}^h}\|w - \varphi\|_{0,\bar{S}_j^h} \leq \left(\sum_T h_T^{2k}|w|_{k,T}^2\right)^{1/2}, \tag{5.8}$$

where T is an element of the mesh $\bar{S}_j^h$, and h_T is the largest side of T. Taking (5.3) into account, it is easy to show that

$$|w|_{k,T}^2 \approx c_1 \int_{r_0 e^{-n\beta_j}}^{r_0 e^{-(n-1)\beta_j}} \rho^{2(\tilde{\alpha}_j - k)}\rho d\rho. \tag{5.9}$$

From (5.8) and (5.9) it becomes evident that we require [30]

$$h_T^{2k}[r_0^{2(\tilde{\alpha}_j-k+1)}e^{2n\beta_j(k-\tilde{\alpha}_j+1)}|1-e^{2(\tilde{\alpha}_j-k+1)\beta_j}|] \approx h^{2k}.$$

By elementary calculations and Taylor's Theorem, it is easy to show that

$$h_T \leq c_2\beta_j r_0 e^{-n\beta_j} + O(\beta^{k+1}).$$

Hence,

$$\begin{aligned}\inf_{\varphi\in\mathcal{V}^h}\|u-\varphi\|_{0,\bar{S}_j^h} &\leq c_3\left(\sum_T \beta_j^{2k} r_0^{2k} e^{-2kn\beta_j} r_0^{2(\tilde{\alpha}_j-k+1)} e^{2n\beta_j(k-\tilde{\alpha}_j+1)}|1-e^{2(\tilde{\alpha}_j-k+1)\beta_j}|\right)^{1/2}\\ &= c_4\sum_T r_0^{\tilde{\alpha}_j+1}\beta_j^k e^{-n\beta_j\tilde{\alpha}_j+1}|1-e^{2(\tilde{\alpha}_j-k+1)\beta_j}|^{1/2}. \end{aligned} \tag{5.10}$$

As $n\beta_j\tilde{\alpha}_j > 0$, where $0 \leq n \leq \nu_j$, it is clear that $e^{-n\beta_j\tilde{\alpha}_j+1} \leq e$. Further, since $k \geq 2$, for $\tilde{\alpha}_j < 1$

$$|1-e^{2(\tilde{\alpha}_j-k+1)\beta_j}| \leq 1,$$

and for $\tilde{\alpha}_j > 1$,

$$|1-e^{2(\tilde{\alpha}_j-k+1)\beta_j}| \leq e^{2(\tilde{\alpha}_j-1)} - 1 = c_5.$$

Hence taking (4.3) into account, from (5.10) we have

$$\inf_{\varphi\in\mathcal{V}^h}\|w-\varphi\|_{0,\bar{S}_j^h} \leq c_6\beta^k \leq c_6 h^k \tag{5.11}$$

for the number of $O(h^{-2}\ln h^{-1})$ spatial elements.

Since there are a finite number of sectors S_j^h, $1 \leq j \leq N$, and since the mesh Ω_h is conforming, it follows from (5.7) and (5.11) that

$$\inf_{\varphi\in\mathcal{V}^h}\|w-\varphi\|_{0,\Omega_h} \leq c_7 h^k. \tag{5.12}$$

Finally, we consider the second term on the right-hand side of (5.6). From (5.2), inequality (5.3) and Schwarz's inequality we have

$$|d(w,z)| \leq c_8\|z\|_{0,\Omega_h}\sum_{j=1}^N r_{j\nu_j}^{\tilde{\alpha}_j}. \tag{5.13}$$

By virtue of (4.4),

$$r_{j\nu_j}^{\tilde{\alpha}_j} = r_{j0}^{\tilde{\alpha}_j} e^{-\nu_j\beta_j\tilde{\alpha}_j} \approx c_9 h^k, \tag{5.14}$$

hence

$$|d(w,z)| \leq c_{10}\|z\|_{0,\Omega_h} h^k. \tag{5.15}$$

From (5.6), (5.12) and (5.15), it follows that

$$\|w - R_h w\|_{0,\Omega_h} \leq ch^k. \tag{5.16}$$

5.1 Error estimation between the solutions of the variational problem and the semi-discrete in space approximation problem

We next consider the error bound between the solutions of problem (4.1)-(4.2) and the corresponding semi-discrete problem (4.7)-(4.8). Let $u(t)$ and $u_h(t)$, $t \in (0,T]$, be the solutions of problems (4.1)-(4.2) and (4.7)-(4.8) respectively.

We first of all write the error as a sum of two terms

$$u_h(t) - u(t) = (u_h(t) - R_h u(t)) + (R_h u(t) - u(t)) = \mu(t) - \rho(t), \tag{5.17}$$

where R_h is the elliptic projection onto $\mathcal{V}^h$ defined by (5.1). Since the Hölder exponent $\widetilde{\alpha}_j$, $1 \le j \le N$, defined in inequality (5.3) is arbitrary, it follows that $\rho(t)$ is bounded as in (5.16). Hence it suffices to bound $\mu(t)$.

From (4.1), (4.7) and the definition of the operator R_h, for $\varphi \in \mathcal{V}^h$ we have

$$\begin{aligned}
(\mu_t, \varphi) + (\nabla \mu, \nabla \varphi) &= (u_{ht}, \varphi) + (\nabla u_{ht}, \nabla \varphi) - (R_h u_t, \varphi) - (\nabla R_h u, \nabla \varphi) \\
&= \frac{1}{\epsilon^2}(f(u_h), \varphi) - (R_h u_t - u_t, \varphi) - (u_t, \varphi) - (\nabla u, \nabla \varphi) \\
&- (\rho, \varphi) - d(w, \varphi) \\
&= -(\rho, \varphi) - (\rho_t, \varphi) + \frac{1}{\epsilon^2}(f(u_h) - f(u), \varphi) - d(w, \varphi).
\end{aligned} \tag{5.18}$$

By a similar argument to the analysis given in [32] (Theorem 14.2, pg. 225), Schwarz's and Sobolev's inequalities,

$$\begin{aligned}
(f(u_h) - f(u), \varphi) &\le c_0 \|u_h - u\|_{0,\Omega_h} \|\varphi\|_{1,\Omega_h} \\
&\le c_1(\|\mu\|_{0,\Omega_h} + \|\rho\|_{0,\Omega_h})(\|\varphi\|_{0,\Omega_h} + \|\nabla \varphi\|_{0,\Omega_h}).
\end{aligned} \tag{5.19}$$

Hence with $\varphi = \mu$, from (5.15), (5.17)-(5.19) and Young's inequality we have

$$\frac{1}{2}\frac{d}{dt}\|\mu\|_{0,\Omega_h} + \|\nabla \mu\|^2_{0,\Omega_h} \le \|\nabla \mu\|^2_{0,\Omega_h} + c_2(\|\mu\|^2_{0,\Omega_h} + \|\rho\|^2_{0,\Omega_h} + \|\rho_t\|^2_{0,\Omega_h}) + ch^{2k}$$

After integration, this shows

$$\|\mu(t)\|^2_{0,\Omega_h} \le ch^{2k} + \|\mu(0)\|^2_{0,\Omega_h} + c_2 \int_0^t (\|\mu\|^2_{0,\Omega_h} + \|\rho\|^2_{0,\Omega_h} + \|\rho_t\|^2_{0,\Omega_h}) ds,$$

and hence using Gronwall's lemma

$$\|\mu(t)\|^2_{0,\Omega_h} \le ch^{2k} + c_3(T)\|\mu(0)\|^2_{0,\Omega_h} + c_4 \int_0^t (\|\rho\|^2_{0,\Omega_h} + \|\rho_t\|^2_{0,\Omega_h}) ds.$$

Using (5.16) together with

$$\|\mu(0)\|_{0,\Omega_h} \le \|u_{h0} - u_0\|_{0,\Omega_h} + \|R_h u_0 - u_0\|_{0,\Omega_h} \le c_5 h^k, \tag{5.20}$$

we have

$$\|u_h(t) - u(t)\|_{0,\Omega_h} \le Ch^k, \tag{5.21}$$

for $t \in (0,T]$, where $C = C(u,T)$.

5.2 Error estimation between the solutions of the variational problem and the fully-discrete approximation problem

We first of all write problem (4.16), (4.17) in the following equivalent weak form: For $u_h^{n-1} \in \mathcal{V}^h$ given, find $u_h^n \in \mathcal{V}^h$ satisfying

$$(\bar{\partial} u_h^n, \varphi) + (\nabla u_h^n, \nabla \varphi) + \frac{\tau}{2\epsilon^2}((\mathcal{H}^{n-1})^2 \bar{\partial} u_h^n, \varphi) = -\frac{1}{\epsilon^2}(\mathcal{H}^{n-1}\mathcal{U}^{n-1}, \varphi), \tag{5.22}$$

$$u_h(0) = u_{h0}, \tag{5.23}$$

for every $\varphi \in \mathcal{V}^h$, where $\bar{\partial} u^n = \frac{u^n - u^{n-1}}{\tau}$.

Let $u(t_n)$ and u_h^n be the solutions of problems (4.1)-(4.2) and (5.22)-(5.23), respectively, at time $t_n = n\tau$, $n = 0, 1, ..., T/\tau$. We consider the upper bound for

$$\|u_h^n - u(t_n)\|_{0,\Omega_h}. \tag{5.24}$$

Following [24] and [32], we decompose the error in the form

$$u_h^n - u(t_n) = (u_h^n - R_h u(t_n)) + (R_h u(t_n) - u(t_n)) = \mu^n + \rho^n,$$

where R_h is the elliptic projection onto $\mathcal{V}^h$ defined by (5.1). Taking into account that the Hölder exponent $\widetilde{\alpha}_j$, $1 \le j \le N$, defined in inequality (5.3) is arbitrary, $\rho^n = \rho(t_n)$ is bounded as (5.16). In order to estimate μ^n, taking (5.22) into account, we note that

$$\begin{aligned}(\bar{\partial}\mu^n, \varphi) + (\nabla \mu^n, \nabla\varphi) + \frac{\tau}{2\epsilon^2}((\mathcal{H}^{n-1})^2 \bar{\partial}\mu^n, \varphi) &= (\bar{\partial} u_h^n, \varphi) + (\nabla u_h^n, \nabla\varphi) \\ &+ \frac{\tau}{2\epsilon^2}((\mathcal{H}^{n-1})^2 \bar{\partial} u_h^n, \varphi) - (\bar{\partial} R_h u(t_n), \varphi) \\ &- (\nabla R_h u(t_n), \nabla\varphi) - \frac{\tau}{2\epsilon^2}((\mathcal{H}^{n-1})^2 \bar{\partial} R_h u(t_n), \varphi).\end{aligned} \tag{5.25}$$

It is easy to see from (5.22) that

$$(\bar{\partial} u_h^n, \varphi) + (\nabla u_h^n, \nabla \varphi) + \frac{\tau}{2\epsilon^2}((\mathcal{H}^{n-1})^2 \bar{\partial} u_h^n, \varphi) = -\frac{1}{\epsilon^2}(\mathcal{H}^{n-1}\mathcal{U}^{n-1}, \varphi), \tag{5.26}$$

and taking (5.1) and the definition of ρ^n into account,

$$\begin{aligned}(\nabla R_h u(t_n), \nabla\varphi) &= a_h(R_h u(t_n), \varphi) - (R_h u(t_n), \varphi) \\ &= (\nabla u(t_n), \nabla\varphi) - (\rho^n, \varphi) + d(u(t_n), \varphi).\end{aligned} \tag{5.27}$$

Furthermore, we have

$$\begin{aligned}(\bar{\partial} R_h u(t_n), \varphi) &= (\bar{\partial} R_h u(t_n) - \bar{\partial} u(t_n), \varphi) + (\bar{\partial} u(t_n), \varphi) \\ &= (\bar{\partial} R_h u(t_n) - \bar{\partial} u(t_n), \varphi) + (\bar{\partial} u(t_n) - u_t(t_n), \varphi) + (u_t(t_n), \varphi).\end{aligned} \tag{5.28}$$

Hence, substituting (5.26)-(5.28) into (5.25), we obtain

$$\begin{aligned}(\bar{\partial}\mu^n, \varphi) + (\nabla \mu^n, \nabla\varphi) + \frac{\tau}{2\epsilon^2}((\mathcal{H}^{n-1})^2 \bar{\partial}\mu^n, \varphi) &= -\frac{1}{\epsilon^2}(\mathcal{H}^{n-1}\mathcal{U}^{n-1}, \varphi) - d(u(t_n), \varphi) \\ &- (\nabla u(t_n), \nabla\varphi) + (\rho^n, \varphi) - (\bar{\partial} R_h u(t_n) - \bar{\partial} u(t_n), \varphi) - (\bar{\partial} u(t_n) - u_t(t_n), \varphi) \\ &- (u_t(t_n), \varphi) - \frac{\tau}{2\epsilon^2}((\mathcal{H}^{n-1})^2 \bar{\partial} R_h u(t_n), \varphi),\end{aligned} \tag{5.29}$$

so that

$$
\begin{aligned}
(\bar{\partial}\mu^n,\varphi)+(\nabla\mu^n,\nabla\varphi)+\frac{\tau}{2\epsilon^2}((\mathcal{H}^{n-1})^2\bar{\partial}\mu^n,\varphi) &= -\frac{1}{\epsilon^2}(\mathcal{H}^{n-1}\mathcal{U}^{n-1},\varphi)-d(u(t_n),\varphi)\\
&-\frac{1}{\epsilon^2}(f(u(t_n)),\varphi)-(\bar{\partial}\rho^n,\varphi)+(\rho^n,\varphi)-(\bar{\partial}u(t_n)-u_t(t_n),\varphi)\\
&-\frac{\tau}{2\epsilon^2}((\mathcal{H}^{n-1})^2\bar{\partial}R_h u(t_n),\varphi).
\end{aligned}
\tag{5.30}
$$

As $\mathcal{H}^n=\frac{-f(u_h^n)}{\sqrt{F(u_h^n)+1}}$, we have

$$
\begin{aligned}
-\frac{1}{\epsilon^2}(\mathcal{H}^{n-1}\mathcal{U}^{n-1},\varphi)-\frac{1}{\epsilon^2}(f(u(t_n)),\varphi) &= \frac{1}{\epsilon^2}\left(\frac{f(u_h^{n-1})}{\sqrt{F(u_h^{n-1})+1}}\mathcal{U}^{n-1},\varphi\right)\\
&-\frac{1}{\epsilon^2}\left(\frac{f(u(t_n))}{\sqrt{F(u(t_n))+1}}\sqrt{F(u(t_n))+1},\varphi\right)\\
&=\frac{1}{\epsilon^2}\left(\frac{f(u_h^{n-1})}{\sqrt{F(u_h^{n-1})+1}}\mathcal{U}^{n-1}-\frac{f(u_h^{n-1})}{\sqrt{F(u_h^{n-1})+1}}\mathcal{U}(u_h^{n-1}),\varphi\right)\\
&+\frac{1}{\epsilon^2}\left(\frac{f(u_h^{n-1})}{\sqrt{F(u_h^{n-1})+1}}\mathcal{U}(u_h^{n-1})\right.\\
&\left.-\frac{f(u(t_n))}{\sqrt{F(u(t_n))+1}}\sqrt{F(u(t_n))+1},\varphi\right).
\end{aligned}
\tag{5.31}
$$

For the first bracketed term on the right-hand side of (5.31) we have

$$
\left(-\mathcal{H}^{n-1}(\mathcal{U}^{n-1}-\mathcal{U}(u_h^{n-1})),\varphi\right)\le\left\|\mathcal{H}^{n-1}\right\|_{L^\infty,\Omega_h}\|\varphi\|_{0,\Omega_h}\|\mathcal{U}^{n-1}-\mathcal{U}(u_h^{n-1})\|_{0,\Omega_h}. \tag{5.32}
$$

From Lemma 4.2 in [15] it follows that $\left\|u_h^{n-1}\right\|_{L^\infty,\Omega_h}$ is bounded. Hence, from the boundedness of $\left\|u_h^{n-1}\right\|_{L^\infty,\Omega_h}$, $F(u)\le 0$, and the continuity of f, it can be easily shown that $\left\|\mathcal{H}^{n-1}\right\|_{L^\infty,\Omega_h}$ is also bounded. Using this, from inequality (5.32) we obtain

$$
\left(-\mathcal{H}^{n-1}(\mathcal{U}^{n-1}-\mathcal{U}(u_h^{n-1})),\varphi\right)\le c\|\varphi\|_{0,\Omega_h}\|\mathcal{U}^{n-1}-\mathcal{U}(u_h^{n-1})\|_{0,\Omega_h}. \tag{5.33}
$$

By the triangle inequality,

$$
\|\mathcal{U}^{n-1}-\mathcal{U}(u_h^{n-1})\|_{0,\Omega_h}\le\|\mathcal{U}^{n-1}-\mathcal{U}(u(t_{n-1}))\|_{0,\Omega_h}+\|\mathcal{U}(u(t_{n-1}))-\mathcal{U}(u_h^{n-1})\|_{0,\Omega_h}. \tag{5.34}
$$

Then from Theorem 4.3 in [15], it follows that

$$
\|\mathcal{U}^{n-1}-\mathcal{U}(u(t_{n-1}))\|_{0,\Omega_h}\le c_0\tau. \tag{5.35}
$$

Next, by the argument presented in the proof of Lemma 3.1 in [15], we have

$$\begin{aligned}\|\mathcal{U}(u(t_{n-1})) - \mathcal{U}(u_h^{n-1})\|_{0,\Omega_h} &\le c_1\|u(t_{n-1}) - u_h^{n-1}\|_{0,\Omega_h} \\ &\le c_2(\|\mu^{n-1}\|_{0,\Omega_h} + \|\rho^{n-1}\|_{0,\Omega_h}).\end{aligned} \tag{5.36}$$

Finally taking the definition of $\mathcal{U}$ and [32] (pg. 225) into account, the second bracketed term on the right-hand side of (5.31) satisfies the inequality

$$|(f(u_h^{n-1}) - f(u(t_n)), \varphi)| \le c_3(\|\mu^{n-1}\|_{0,\Omega_h} + \|\rho^{n-1}\|_{0,\Omega_h} + \tau\|\bar{\partial}u(t_n)\|_{0,\Omega_h})(\|\varphi\|_{0,\Omega_h} + \|\nabla\varphi\|_{0,\Omega_h}). \tag{5.37}$$

We will also need the following estimates which can be calculated easily. By virtue of assumption (2.7), and since the operator R_h commutes with time differentiation, from inequality (5.16) we have the error estimate

$$\|\rho_t^n\|_{0,\Omega_h} = \|R_h u_t(t_n) - u_t(t_n)\|_{0,\Omega_h} \le ch^k,$$

so that

$$\|\bar{\partial}\rho^n\|_{0,\Omega_h} = \|\tau^{-1}\int_{t_{n-1}}^{t_n} \rho_t ds\|_{0,\Omega_h} \le ch^k. \tag{5.38}$$

Furthermore, taking assumption (2.8) into account, ([32], pg. 216),

$$\|\bar{\partial}u(t_n) - u_t(t_n)\|_{0,\Omega_h} \le \|\tau^{-1}\int_{t_{n-1}}^{t_n} (s - t_{n-1})u_{tt}(s)ds\|_{0,\Omega_h} \le c(u)\tau, \tag{5.39}$$

and by the Schwarz and triangle inequalities,

$$\begin{aligned}-\frac{\tau}{2\epsilon^2}((\mathcal{H}^{n-1})^2\bar{\partial}R_h u(t_n), \varphi) &\le \frac{\tau}{2\epsilon^2}\|(\mathcal{H}^{n-1})^2\|_{L^\infty,\Omega_h}\|\bar{\partial}R_h u(t_n)\|_{0,\Omega_h}\|\varphi\|_{0,\Omega_h} \\ &\le c\frac{\tau}{2\epsilon^2}\|\varphi\|_{0,\Omega_h}\frac{1}{\tau}\left(\|R_h u(t_n) - R_h u(t_{n-1})\|_{0,\Omega_h}\right) \\ &\le \frac{c}{2\epsilon^2}\|\varphi\|_{0,\Omega_h}\big(\|R_h u(t_n) - u(t_n)\|_{0,\Omega_h} \\ &\quad + \|u(t_{n-1}) - R_h u(t_{n-1})\|_{0,\Omega_h} + \tau\|\bar{\partial}u(t_n)\|_{0,\Omega_h}\big) \\ &\le c(u)\|\varphi\|_{0,\Omega_h}(h^k + \tau).\end{aligned} \tag{5.40}$$

Combining (5.15), (5.31)-(5.40) and letting $\varphi = \mu^n$, with the application of Schwarz's and Young's inequalities we have

$$(c + c_4\tau/\epsilon^2)\bar{\partial}\|\mu^n\|_{0,\Omega_h}^2 \le c_5\|\mu^{n-1}\|_{0,\Omega_h}^2 + c_6(u)(h^k + \tau)^2, \tag{5.41}$$

or

$$\|\mu^n\|_{0,\Omega_h}^2 \le \frac{c + c_4\tau/\epsilon^2 + c_5\tau}{c + c_4\tau/\epsilon^2}\|\mu^{n-1}\|_{0,\Omega_h}^2 + \tau c_7(u)(h^k + \tau)^2. \tag{5.42}$$

Whence by repeated application,

$$\|\mu^n\|^2_{0,\Omega_h} \leq c_8(u)\|\mu^0\|^2_{0,\Omega_h} + c_9(u)(h^k + \tau)^2. \tag{5.43}$$

Since

$$\|\mu^0\|_{0,\Omega_h} \leq \|u_{h0} - u(t_0)\| + \|u(t_0) - R_h u(t_0)\| \leq c_{10} h^k,$$

we have

$$\|u_h^n - u(t_n)\|_{0,\Omega_h} \leq C(u)(h^k + \tau). \tag{5.44}$$

Remark 2. *For physical significance, the prescribed constant ϵ may be small and this raises the question of how the constants in estimates (5.21) and (5.44) depends on the width of the interface. In this paper we have not considered this problem and have done the error analysis under the assumption that ϵ is fixed. However, a closer examination of the arguments in Sections 5.1 and 5.2 indicates that the constants may depend on ϵ exponentially because of the use of the Gronwall inequality [34].*

6 Numerical Simulations

In this section we demonstrate the numerical results obtained for the numerical solution of problem (2.1)-(2.3) from the corresponding discrete problem (4.16), (4.17). The numerical examples are solved in the L-Shaped domain denoted by Ω with boundary γ, where

$$\Omega = \{(x, y) : -1 < x < 1, -1 < y < 1\}\backslash\Omega_1, \tag{6.1}$$

$\Omega_1 = \{(x, y) : 0 \leq x \leq 1, -1 \leq y \leq 0\}$, so that the domain has a re-entrant corner with an interior angle $\omega_1 = 3\pi/2$ at the origin.

In each of the examples, the initial condition is chosen so that the interface intersects the singular corner of the domain for some $t_n = n\tau \in (0, T)$, where the time-step has the fixed value $\tau = 0.001$.

For the implementation of the method, linear Lagrange elements were employed for spatial discretization, so that an accuracy of $O(h^2 + \tau)$ is expected in the L^2-norm, where h is the spatial mesh step defined as in Section 4. Since the solution only has a weak singularity in the neighbourhood of convex corners and the given boundary data is continuous on γ, we only need to apply exponentially refined meshes in the vicinity of the re-entrant corner at the origin for an accuracy of $O(h^2)$ in space, in the L^2-norm. The calculations were carried out in *Matlab R2017a*, by customizing the package *p1afem* [33] for the implementation of the finite element method.

The exact solutions of the solved problems are not known. Hence we present the spatial convergence rate of the numerical solution at different time steps, where the interface intersects the singular corner, by comparing the numerical solution attained on the sector S_1^h in the neighbourhood of the singular corner on successive grids. The radius of the sector is $r_{10} = 0.5$ for both of the examples. The convergence rate in space at the time step $t = n\tau$, on the grid with $h = 2^{-m}$, $m = 4, 5, 6$, is defined as

$$\mathcal{E}^n_{2^{-m}} = \frac{\|u^n_{2^{-(m+1)}} - u^n_{2^{-m}}\|_{0,S_1^h}}{\|u^n_{2^{-(m+1)}} - u^n_{2^{-(m+2)}}\|_{0,S_1^h}}, \tag{6.2}$$

$(2^{-m},\nu_1)$	$\mathcal{E}^3_{2^{-m}}$	$\mathcal{E}^{14}_{2^{-m}}$
$(2^{-4},200)$		
$(2^{-5},400)$		
$(2^{-6},800)$	3.6770	3.9762

$\epsilon = 0.05$

$(2^{-m},\nu_1)$	$\mathcal{E}^3_{2^{-m}}$	$\mathcal{E}^{14}_{2^{-m}}$
$(2^{-4},260)$		
$(2^{-5},520)$		
$(2^{-6},1040)$	3.0230	4.0958

$\epsilon = 0.03$

$(2^{-m},\nu_1)$	$\mathcal{E}^3_{2^{-m}}$	$\mathcal{E}^{14}_{2^{-m}}$
$(2^{-4},260)$		
$(2^{-5},520)$		
$(2^{-6},1040)$	3.1125	4.8706

$\epsilon = 0.025$

Table 1: The convergence rate in space of the numerical solution to problem (6.3)-(6.5) on successive grids at $t = 0.003$ and $t = 0.014$ for decreasing values of ϵ.

where the $O(h^2)$ accuracy corresponds to 2^2 for the spatial convergence rate. The value of ν_1 is chosen such that the number of element nodes are consistent on each successive grid.

Example 1. *Consider the problem*

$$u_t - \Delta u = \frac{1}{\epsilon^2} f(u) \text{ in } \Omega \times (0,T], \tag{6.3}$$

$$\frac{\partial u}{\partial n} = 0 \text{ on } \gamma \times (0,T], \tag{6.4}$$

$$u(\boldsymbol{x},0) = u_0(\boldsymbol{x}) \text{ in } \Omega, \tag{6.5}$$

where the function f is defined as in (2.4) and $u_0(\boldsymbol{x}) = \tanh\left(\frac{0.35-\sqrt{(x-0.35)^2+y^2}}{\sqrt{2}\epsilon}\right)$ is the initial condition. It is well-known that such a circular interface is unstable, and as time increases it will shrink and eventually dissapear [5]. This is also demonstrated in the numerical simulation of the solution for problem (6.3)-(6.5) in Figure 2. The convergence rates in space (6.2), at $t = 0.003$ and $t = 0.014$ and the spatial mesh pairs (h,ν_1) are presented in Table 1 for decreasing values of the width of the interface ϵ. As it can be observed from the simulations of the solutions presented in Figure 3, the interface intersects the singular corner at these time steps.

Example 2. *Consider the problem*

$$u_t - \Delta u = \frac{1}{\epsilon^2} f(u) \text{ in } \Omega \times (0,T], \tag{6.6}$$

$$\frac{\partial u}{\partial n} = 0 \text{ on } \gamma \times (0,T], \tag{6.7}$$

$$u(\boldsymbol{x},0) = u_0(\boldsymbol{x}) \text{ in } \Omega, \tag{6.8}$$

where f is defined as in (2.4) and $u_0(\boldsymbol{x}) = \tanh\left(\frac{0.35-\sqrt{(x-0.15)^2+y^2}}{\sqrt{2}\epsilon}\right)$ is the initial condition. From Figure 4 it can be seen that the interface moves into the singular corner as time increases and it continually shrinks. The convergence rates in space of the numerical solution on successive grids in the sector S_1^h are given at time steps $t = 0.035$

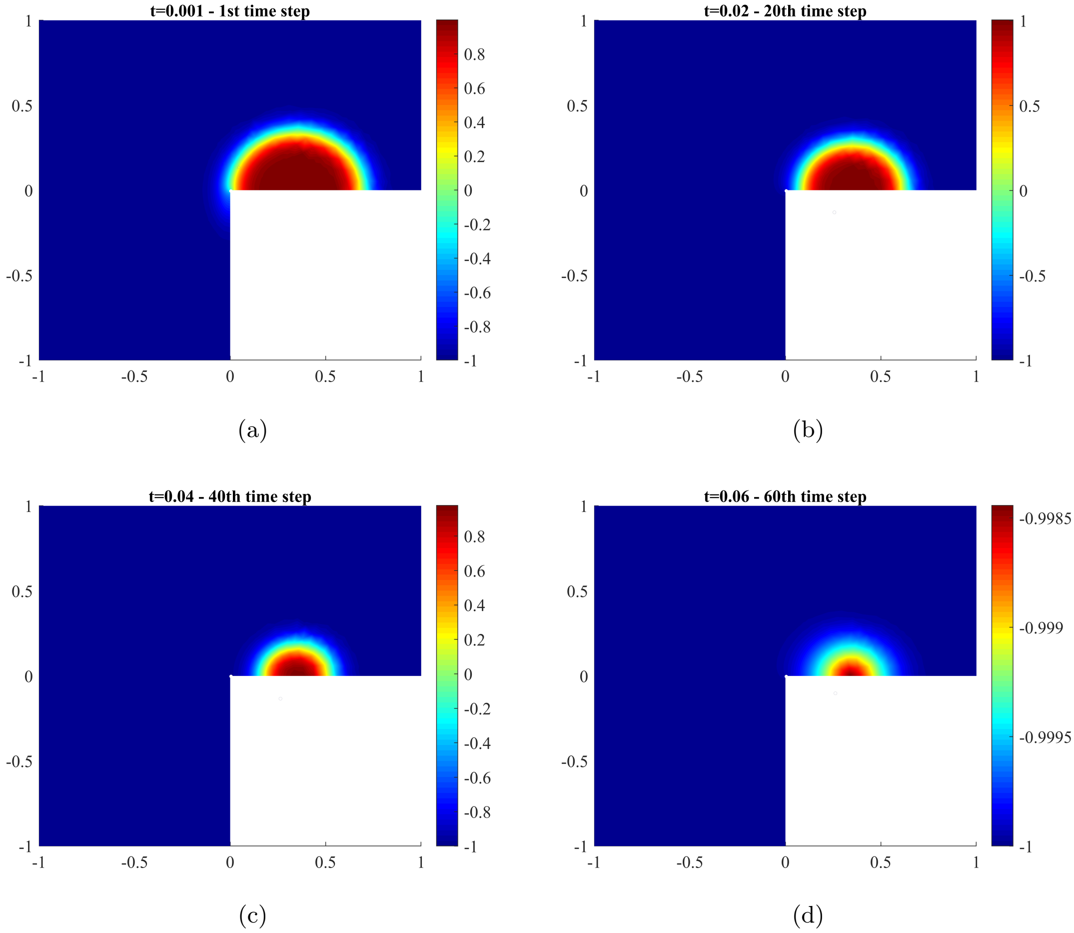

Figure 2: The numerical solution of Example 1 for $\epsilon = 0.05$ at various time steps.

and $t = 0.043$ *for* $\epsilon = 0.05, 0.03,$ *and at* $t = 0.015$ *and* $t = 0.021$ *for* $\epsilon = 0.025$ *in Table 2. At these time steps, the interface is intersecting the singular corner. This intersection is illustrated in Figure 5 for* $\epsilon = 0.05$.

We have also considered the polluting effect of the corner singularity in Example 1 with $\epsilon = 0.5$, by taking into account the approximate solution obtained on a structured mesh, where the mesh size for each triangle was fixed to h. Calculating the rate of convergence $\mathcal{E}^n_{2^{-m}}$ by formula (6.2) for $h = 2^{-m}$, $m = 4, 5, 6$, on an extended time interval, it was noted that $\mathcal{E}^n_{2^{-m}}$, $n = 1, 2, ..., 800$, was approximately equal to 3.2 while the interface was present in the solution, so that the order of convergence was reduced to 1.68. The reduced rate was not observed after the interface vanished. As this reduction is a consequence of the corner singularity, the use of higher order basis functions will not improve the accuracy of the approximate solution.

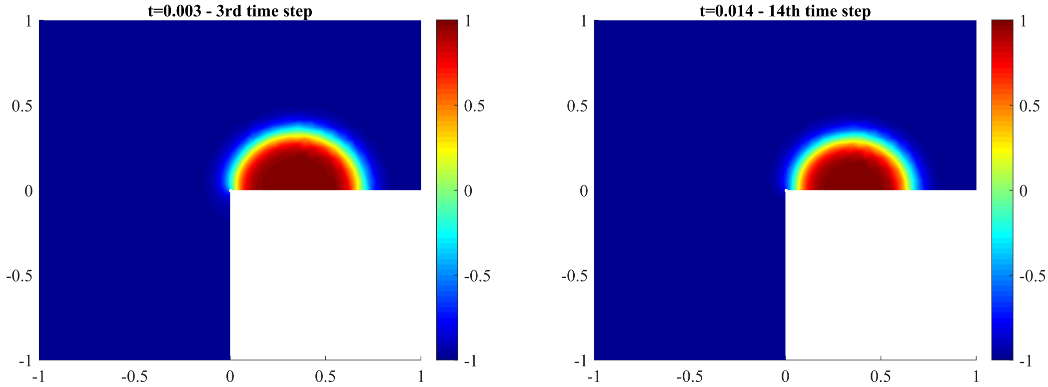

(a) (b)

Figure 3: The numerical solution of Example 1 for $\epsilon = 0.05$ at two time-steps where the interface intersects with the singular corner.

$(2^{-m}, \nu_1)$	$\mathcal{E}^{35}_{2^{-m}}$	$\mathcal{E}^{43}_{2^{-m}}$	$(2^{-m}, \nu_1)$	$\mathcal{E}^{35}_{2^{-m}}$	$\mathcal{E}^{43}_{2^{-m}}$	$(2^{-m}, \nu_1)$	$\mathcal{E}^{15}_{2^{-m}}$	$\mathcal{E}^{21}_{2^{-m}}$
$(2^{-4}, 300)$			$(2^{-4}$,300)			$(2^{-4}$,340)		
$(2^{-5}, 600)$			$(2^{-5}$,600)			$(2^{-5}$,680)		
$(2^{-6}, 1200)$	3.8876	3.7188	$(2^{-6}$,1200)	3.7924	3.9801	$(2^{-6}$,1360)	5.0206	3.7693

$\epsilon = 0.05$ $\epsilon = 0.03$ $\epsilon = 0.025$

Table 2: The convergence rate in space of the numerical solution to problem (6.6)-(6.8) on successive grids at $t = 0.035$ and $t = 0.043$ for $\epsilon = 0.05$ and $\epsilon = 0.03$, and at $t = 0.015$ and $t = 0.021$ for $\epsilon = 0.025$

7 Concluding Remarks

In this paper, to overcome the effect of the corner singularities on the accuracy of the approximate solution, which are acquired by the solution at the intersection of the interface with the corners of the polygon, for spatial discretization we have developed an efficient finite element mesh with exponentially compressed polar meshes in the vicinity of the singular corners, and applied the finite element method based on the $(k-1)th$ order Lagrange elements .

To fully discretize the problem, a first-order time stepping scheme with the unconditionally energy stable Invariant Energy Quadratization (IEQ) approach has been employed in time, and the use of this method for the finite element solution of the problem has been analyzed.

It has been shown that the numerical solution has an order of accuracy of $O(h^k + \tau)$ in the L^2-Norm for the number of $O(h^{-2} \ln h^{-1})$ elements in space, $k \geq 2$ an integer, where h and τ are the mesh and time steps respectively. The numerical results obtained

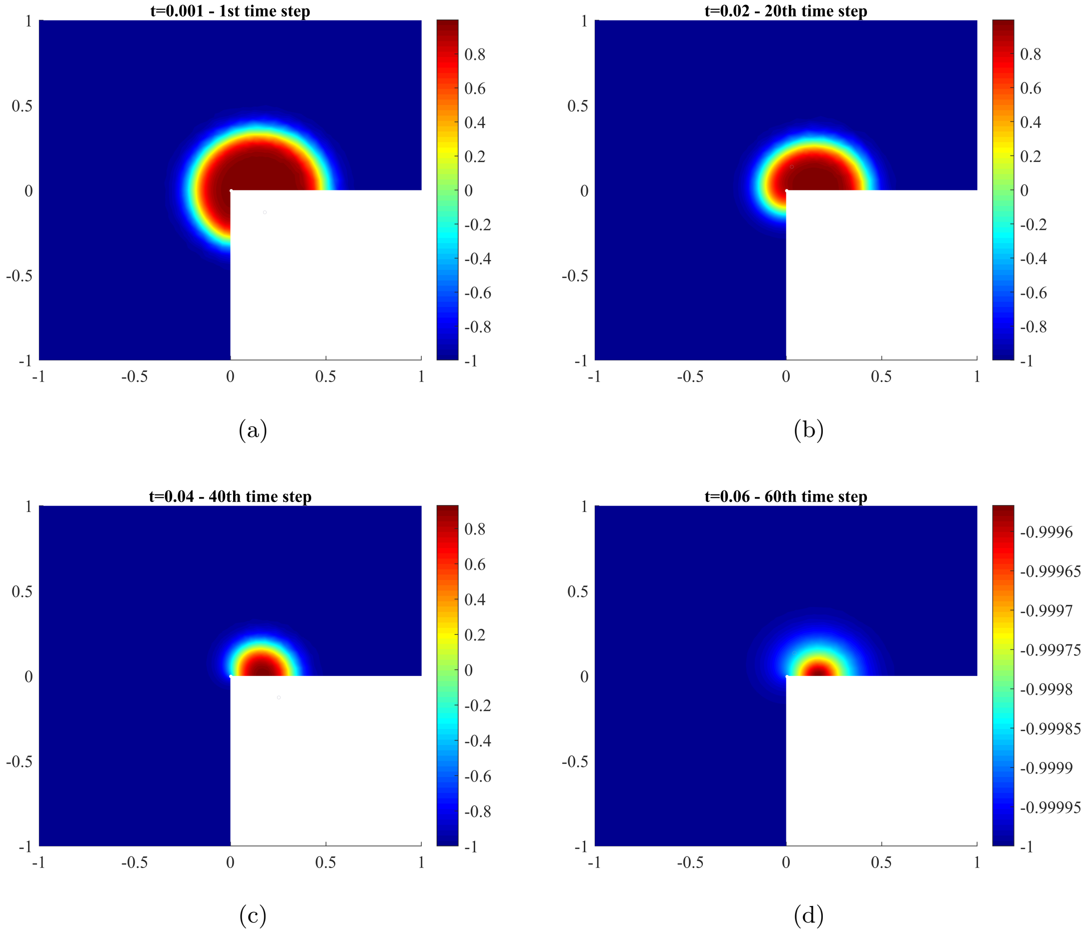

Figure 4: The numerical solution of problem Example 2 for $\epsilon = 0.05$ at different time steps.

support the analysis made.

A non-trivial extension of these results will be to further extend the constructed method for the numerical solution of the Allen-Cahn equation in three-dimensional, polyhedral domains. The results can also be extended for obtaining the approximate solution of two-phase flow problems by taking into account the system of equations formed by the coupled Navier-Stokes and Allen-Cahn equations in domains with sharp or re-entrant corners.

The application of the constructed method is not restricted to the Allen-Cahn equation and can be employed for the numerical solutions of all second-order singular perturbation equations satisfying the conditions outlined in Section 2.

Since corner singularities reduce the accuracy of the approximate solution due to the bounds on the spatial derivatives of the exact solution, employing a temporally second-

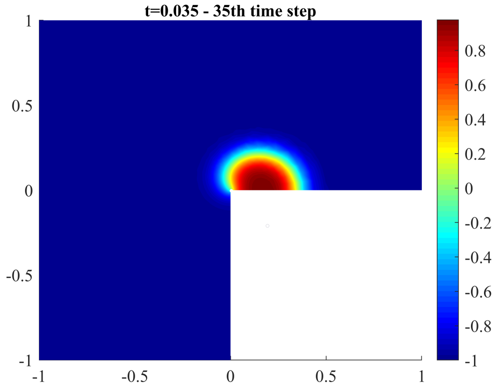

(a)

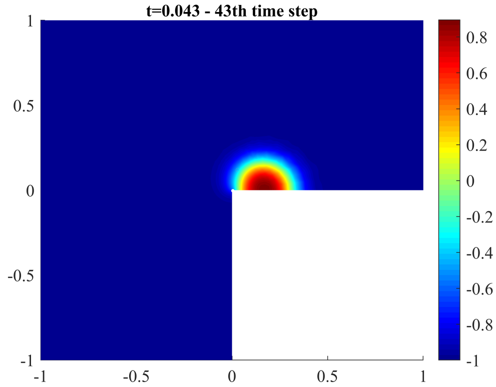

(b)

Figure 5: The numerical solution of Example 2 for $\epsilon = 0.05$ at two time-steps where the interface intersects with the singular corner.

order accurate scheme with the method described above would increase the solution's accuracy to $O(h^k + \tau^2)$.

Acknowledgements

E. Celiker's work is supported by the EU Scholarship Programme for the Turkish Cypriot Community 2017/18. This study was mostly completed while E. Celiker was at the University of Dundee.

References

[1] Allen, S. M., and Cahn, J. W. (1979). A microscopic theory for antiphase boundary motion and its application to antiphase domain coarsening. *Acta Metallurgica*, 27(6), 1085-1095.

[2] Chen, L. Q. (2002). Phase-field models for microstructure evolution. *Annual review of materials research*, 32(1), 113-140.

[3] Kohn, R. V., and Sternberg, P. (1989). Local minimisers and singular perturbations. *Proceedings of the Royal Society of Edinburgh Section A: Mathematics*, 111(1-2), 69-84.

[4] Iron, D., Kolokolonikov, T., Rumsey, J., and Wei, J. (2009). Stability of curved interfaces in the perturbed two-dimensional allen-cahn system. *SIAM Journal on Applied Mathematics*, 69(5), 1228-1243.

[5] Zhang, J., and Du, Q. (2009). Numerical studies of discrete approximations to the Allen-Cahn equation in the sharp interface limit. *SIAM Journal on Scientific Computing*, 31(4), 3042-3063.

[6] Jeong, D., Lee, S., Lee, D., Shin, J., and Kim, J. (2016). Comparison study of numerical methods for solving the Allen-Cahn equation. *Computational Materials Science*, 111, 131-136.

[7] Shen, J., and Yang, X. (2010). Numerical approximations of allen-cahn and cahn-hilliard equations. *Discrete Contin. Dyn. Syst*, 28(4), 1669-1691.

[8] Gong, Y., Zhao, J., and Wang, Q. (2017). Linear second order in time energy stable schemes for hydrodynamic models of binary mixtures based on a spatially pseudospectral approximation. *Advances in Computational Mathematics*, 1-28.

[9] Shen, J., Xu, J., and Yang, J. (2017). A new class of efficient and robust energy stable schemes for gradient flows. arXiv preprint arXiv:1710.01331.

[10] Kelong Cheng, Cheng Wang and Steven M. Wise (2019). An Energy Stable BDF2 Fourier Pseudo-Spectral Numerical Scheme for the Square Phase Field Crystal Equation *Communications in Computational Physics*, 26, 1335-1364.

[11] Jon Matteo Church, Zhenlin Guo, Peter K. Jimack, Anotida Madzvamuse, Keith Promislow, Brian Wetton, Steven M. Wise and Fengwei Yang (2019). High accuracy benchmark problems for Allen-Cahn and Cahn-Hilliard dynamics. *Communications in Computational Physics*, 26(4), 947-972.

[12] Yan, Y., Chen, W., Wang, C. and Wise, S. M. (2018). A second-order energy stable BDF numerical scheme for the Cahn-Hilliard equation. *Communications in Computational Physics*, 23(2), 572-602.

[13] Lee, S., and Kim, J. (2019). Effective Time Step Analysis of a Nonlinear Convex Splitting Scheme for the Cahn–Hilliard Equation. *Communications in Computational Physics*, 25(2), 448-460.

[14] Yang, X. (2016). Linear, first and second-order, unconditionally energy stable numerical schemes for the phase field model of homopolymer blends. *Journal of Computational Physics*, 327, 294-316.

[15] Yang, X., and Zhang, G. (2017). Numerical approximations of the Cahn-Hilliard and Allen-Cahn Equations with general nonlinear potential using the Invariant Energy Quadratization approach. arXiv preprint arXiv:1712.02760

[16] Feng, X., and Wu, H. J. (2005). A posteriori error estimates and an adaptive finite element method for the Allen–Cahn equation and the mean curvature flow. *Journal of Scientific Computing*, 24(2), 121-146.

[17] Li, Z. C., and Lu, T. T. (2000). Singularities and treatments of elliptic boundary value problems. *Mathematical and Computer Modelling*, 31(8-9), 97-145.

[18] Dobrowolski, M. (1985). On finite element methods for nonlinear elliptic problems on domains with corners. *In Singularities and Constructive Methods for Their Treatment* (pp. 85-103). Springer, Berlin, Heidelberg.

[19] Volkov, E. A. (1976). The method of composite regular nets for the Laplace equation on polygons. *Trudy Mat. Inst. Steklov.*, 140, 68-102 (Russian), translation in Proc. Steklov Inst. Math., 140 (1979), 71-109.

[20] Dosiyev, A. A. (2002) *A fourth-order accurate composite grid method for solving Laplace's boundary value problems with singularities.* Zh. Vychisl. Mat. Mat. Fiz., 42(6), 867-884.

[21] Volkov, E. A., and Dosiyev, A. A. (2007) *A high accurate composite grid method for solving Laplace's boundary value problems with singularities.* Russian Journal of Numerical Analysis and Mathematical Modelling, 22(3), 291-307.

[22] Celiker, E., and Lin, P. (2019). *A highly-accurate finite element method with exponentially compressed meshes for the solution of the Dirichlet problem of the generalized Helmholtz equation with corner singularities.* Journal of Computational and Applied Mathematics, 361, 227-235.

[23] Temam, R. (1991). Stability analysis of the nonlinear Galerkin method. *mathematics of computation*, 57(196), 477-505.

[24] Wheeler, M. F. (1973). A priori L_2 error estimates for Galerkin approximations to parabolic partial differential equations. *SIAM Journal on Numerical Analysis*, 10(4), 723-759.

[25] Chatzipantelidis, P., Lazarov, R. D., Thomé, V., and Wahlbin, L. B. (2006). Parabolic finite element equations in nonconvex polygonal domains. *BIT Numerical Mathematics*, 46(1), 113-143.

[26] Brenner, S., and Scott, R. (2007). *The mathematical theory of finite element methods* (Vol. 15). Springer Science Business Media.

[27] Zlámal, M. (1973) Curved elements in the finite element method I. *SIAM Journal on Numerical Analysis*, 10(1), 229-240.

[28] Zláman, M. (1974) Curved elements in the finite element method II. *SIAM Journal on Numerical Analysis*, 11(2), 347-362.

[29] Zlámal, M. (1973) The finite element method in domains with curved boundaries. *International Journal for Numerical Methods in Engineering*, 5(3), 367-373.

[30] Burda, P., Novotný, J., and S̃ístek, J. (2005). Precise FEM solution of a corner singularity using an adjusted mesh. *International journal for numerical methods in fluids*, 47(10-11), 1285-1292.

[31] Harrell, E. M., and Layton, W. J. (1987). L^2 Estimates for Galerkin Methods for Semilinear Elliptic Equations. *SIAM journal on numerical analysis*, 24(1), 52-58.

[32] Thomée, V. (1984). *Galerkin finite element methods for parabolic problems* (Vol. 1054). Berlin: Springer-Verlag.

[33] Funken, S., Praetorius, D., and Wissgott, P. (2011). Efficient implementation of adaptive P1-FEM in Matlab. *Computational Methods in Applied Mathematics*, 11(4), 460-490.

[34] Feng, X., and Prohl, A. (2004). Analysis of a fully discrete finite element method for the phase field model and approximation of its sharp interface limits. *Mathematics of computation*, 73(246), 541-567.